Supporting Information

Hierarchical NiCo-LDH/NiCoP@NiMn-LDH Hybrid Electrodes on Carbon Cloth for Excellent Supercapacitors

Haoyan Liang, Jinghuang Lin, Henan Jia, Shulin Chen, Junlei Qi*, Jian Cao*,

Tiesong Lin*, Weidong Fei and Jicai Feng

State Key Laboratory of Advanced Welding and Joining, Harbin Institute of Technology, Harbin 150001, China

*Corresponding authors: Tel. /fax: 86-451-86418146;

E-mail: jlqi@hit.edu.cn (J. Qi)

Experimental Section

Synthesis of NiCo-LDH nanowires on carbon cloth. In a typical procedure, A piece of carbon cloth (2.0 cm × 5.0 cm) was cleaned in 10% HCl with an ultrasound treatment for 10 min to remove the surface oxides and rinsed with ethanol and deionized water. 6 mmol of $CoCl_2 \cdot 6H_2O$, 3 mmol of $NiCl_2 \cdot 6H_2O$ and 18 mmol of urea were dissolved in 60 mL of deionized water to form a homogenous solution. The cleaned carbon cloth was immersed into the solution and then the solution was transferred into a 100 mL Teflon-lined stainless steel autoclave. The autoclave was sealed and maintained at 120 ^oC for 8 h. The resulting product was washed with deionized water and ethanol for several times and dried overnight.

Synthesis of the NiCo-LDH/NiCoP (Denoted by NCLP) nanowires. To prepare the NiCo-LDH/NiCoP nanowires, the method of chemical vapor deposition was used. The NiCo-LDH precursor was placed on a piece of glass with $NaH_2PO_2 \cdot H_2O$ powder (300 mg) at the upstream. After that, the tube furnace was heated to 300 ^oC with a 2 $^oC\ min^{-1}$ rate and maintained for 2 h in a flow Ar atmosphere. The NCLP nanowires were obtained when the temperature was cooled down. For comparison, the NiCo-LDH precursor was annealed at the same condition only without phosphorous source.

Synthesis of the NCLP@NiMn-LDH hybrid structure. 1 mmol of $MnCl_2 \cdot 4H_2O$, 3 mmol $NiCl_2 \cdot 6H_2O$ and 5 mmol hexamethylenetetramine were dissolved in 70 mL of deionized water. The carbon cloth with NCLP nanowires was immersed into the prepared solution. Then the homogeneous solution was transferred into 100 mL Teflon-lined stainless steel autoclave and kept at 90 ^oC for 8 h. The sample was rinsed

with deionized water and ethanol for several times and dried at 60 ^{o}C overnight. For comparison, the NiCo-LDH@NiMn-LDH hybrid structure is also prepared under the same condition except the phosphorization process. The mass loading of NCLP@NiMn-LDH and NiCo-LDH@NiMn-LDH are 2.5 mg cm^{-2} and 3.4 mg cm^{-2}, respectively.

Material characterization. X-ray diffraction patterns were collected with D/max 2550 to characterize the crystal structures of materials. The morphologies and microstructures were observed by scanning electron microscope (HELIOS NanoLab 600i) and transmission electron microscope (Tecnai G2 F30). The chemical compositions and chemical valence states of the samples were studied with X-ray photoelectron spectrometer (ESCLAB 250Xi). Thermogravimetric analysis was carried out to confirm the changes during the annealing process. The surface area and pore-size distribution was calculated with the Brunauer-Emmett-Teller (BET) equation and Barrett-Joyner-Halenda (BJH) method.

Electrochemical measurements. Electrochemical measurements were carried out using three-electrode cell in a 6 M KOH electrolyte. The as-prepared sample was used as the working electrode, while the Pt foil was used as the counter electrode. The Hg/HgO acted as the reference electrode. Cyclic voltammetry (CV) and galvanostatic charge/discharge (GCD) curves were conducted on an electrochemical workstation (CHI760E). Electrochemical impedance spectroscopy (EIS) analysis was conducted using the electrochemical workstation (PARSTAT 4000A), ranging from 100 kHz to 0.1 Hz with amplitude of 5 mV.

The asymmetric supercapacitor device was assembled using NCLP@NiMn-LDH and active carbon (AC) as the positive and negative electrode, respectively. The mass loading ratio between two electrodes was calculated according to equation (1). And the corresponding energy density (E) and power density (P) were calculated following equation (2) and (3).

$$m_+/m_- = \Delta V_- C_-/\Delta V_+ C_+ \quad (1)$$

$$E = \int I \times V(t)dt/(3.6M) \quad (2)$$

$$P = 3600 \times E/\Delta t \quad (3)$$

where M presents the total mass of both electrodes (mg).

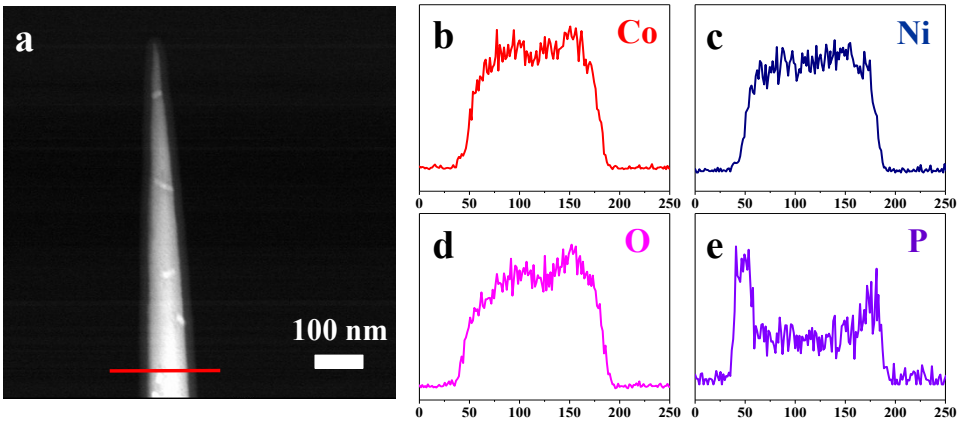

Fig. S1 (a) HAADF images of NCLP and Element line spectrum of (b) Co, (c) Ni, (d) O and (e) P.

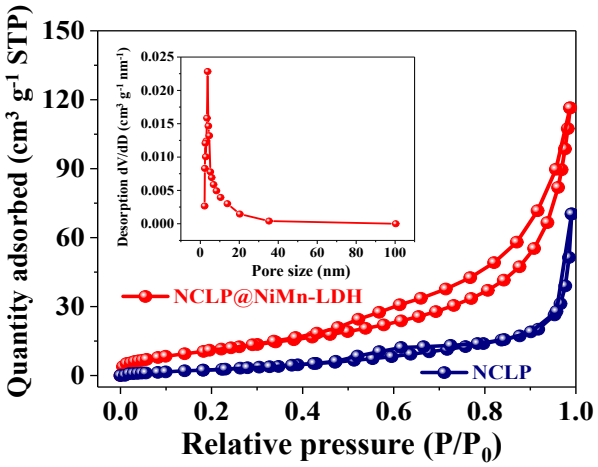

Fig. S2 N_2 adsorption-desorption isotherms and pore size distribution.

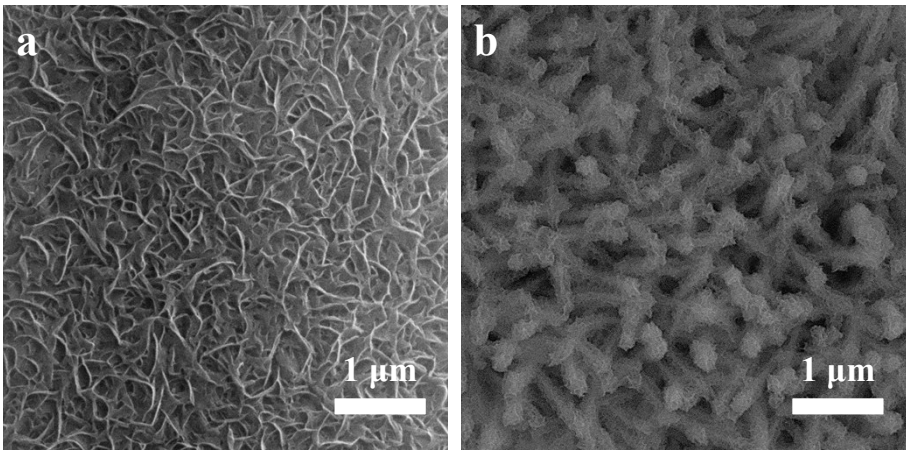

Fig. S3 SEM images of (a) NiMn-LDH and (b) NiCo-LDH@NiMn-LDH core-shell structure.

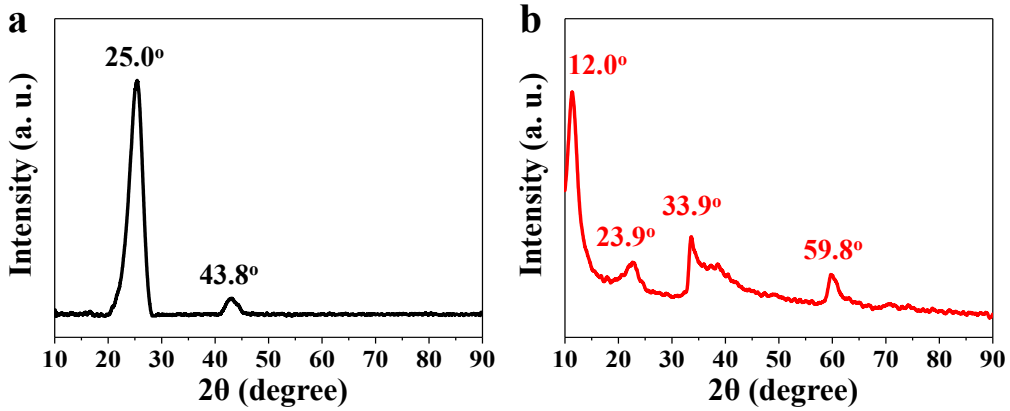

Fig. S4 XRD patterns of (a) Carbon Cloth and (b) NiMn-LDH.

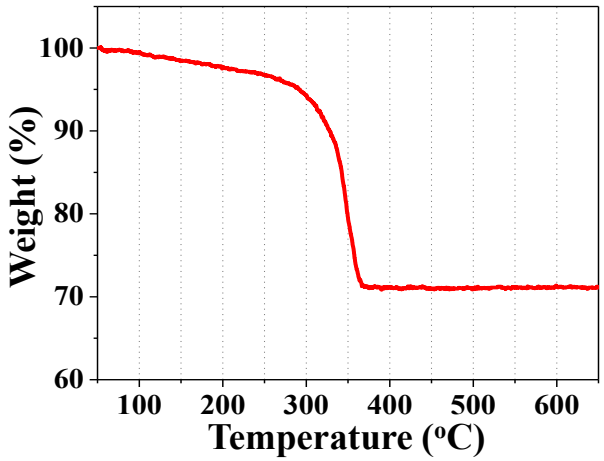

Fig. S5 TG profile for NiCo-LDH precursor under Ar flow at the temperature ramp of 5 °C min^{-1}.

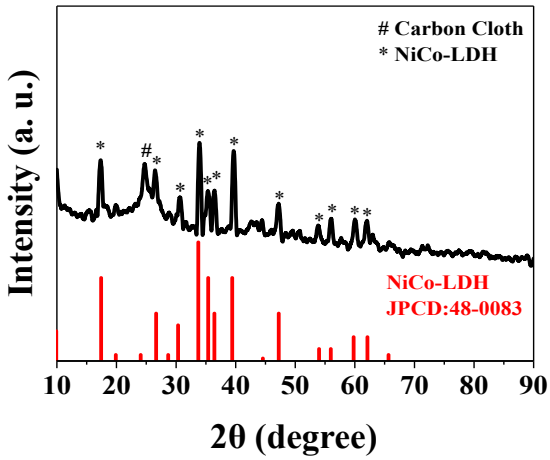

Fig. S6 XRD pattern of annealed NiCo-LDH under the same condition without phosphorus source.

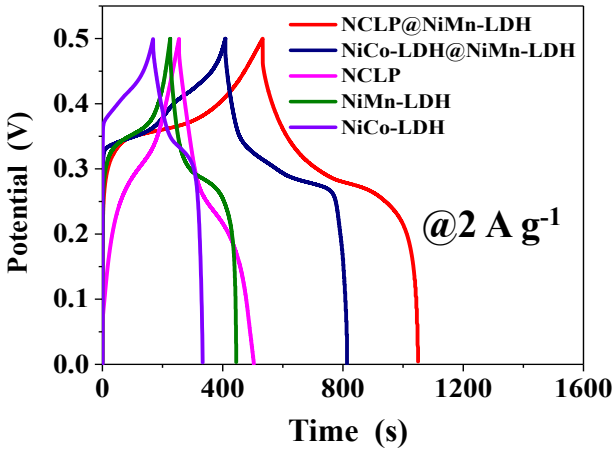

Fig. S7 The comparison of GCD curves of different electrodes at a current density of 2 A g^{-1}.

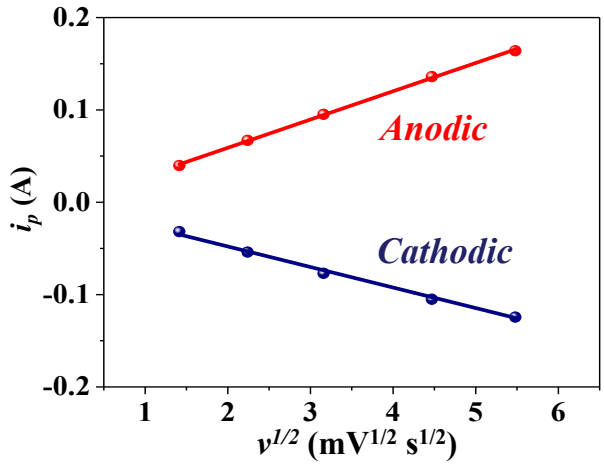

Fig. S8 The corresponding plots of anodic and cathodic peak current vs. scanning rate in NCLP@NiMn-LDH.

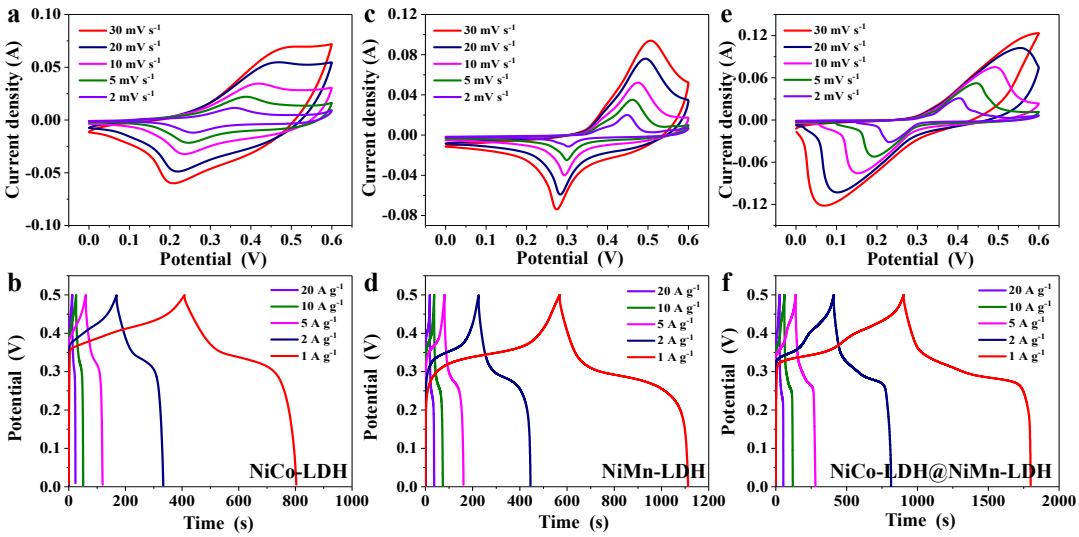

Fig. S9 CV and GCD curves of (a and b) NiCo-LDH, (c and d) NiMn-LDH and (e and f) NiCo-LDH@NiMn-LDH.

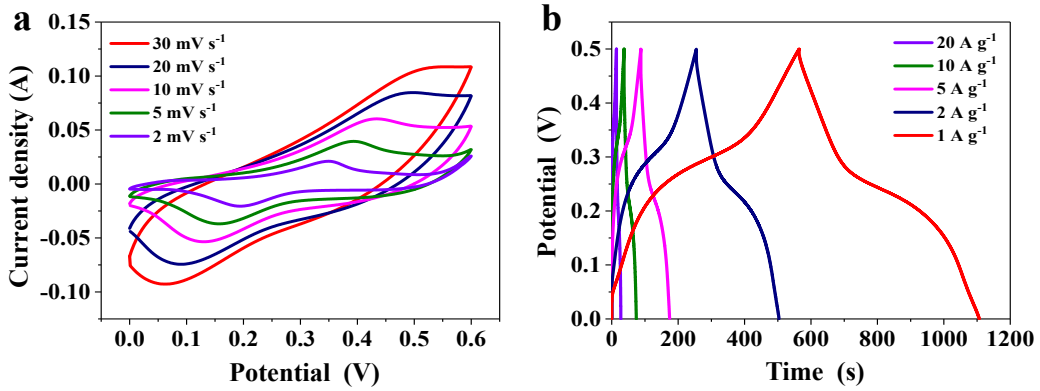

Fig. S10 (a) CV and (b) GCD curves of NCLP.

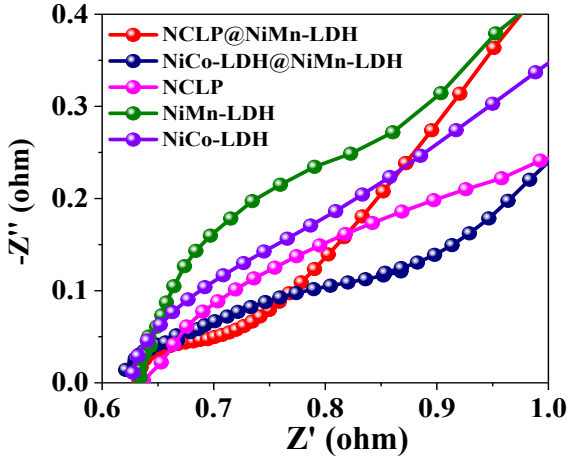

Fig. S11 The magnified plots of EIS in high frequency region.

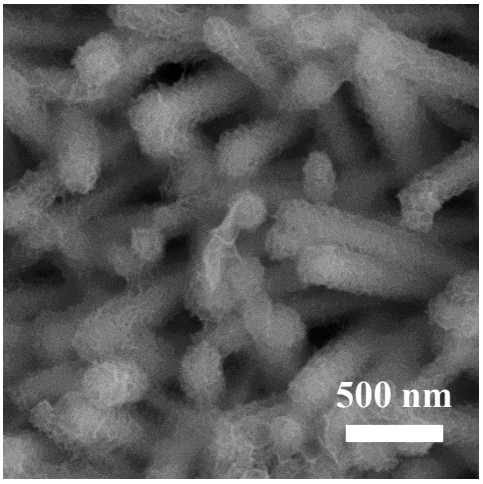

Fig. S12 SEM images of NCLP@NiMn-LDH core-shell structure after 10000 cycles.

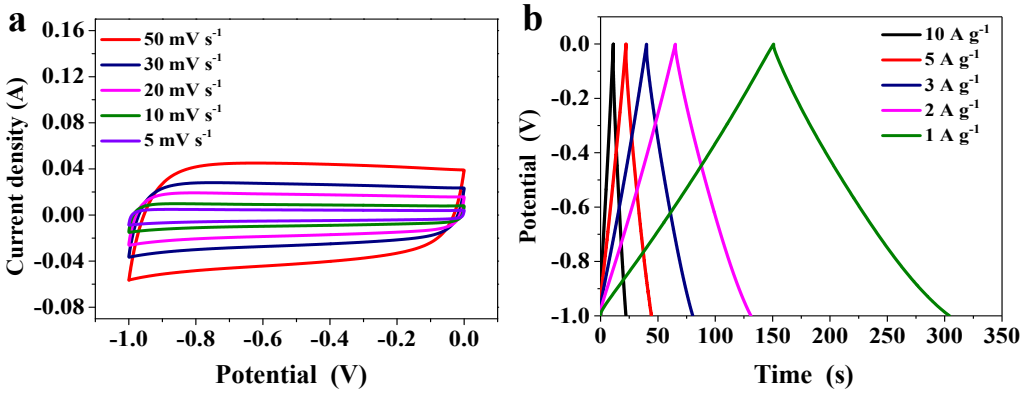

Fig. S13 (a) CV of active carbon at different scanning rates and (b) GCD curves at different current density.

Table S1. The comparison of various electrodes in the three-electrode system in references

electrode materials	specific capacitance	capacitance retention	cycling stability (cycles)	Ref
NiAl LDH nanotubes	2123.7 F g^{-1} (0.5 A g^{-1})	70.7% (20 A g^{-1})	91.9% (10000)	1
Mxene-NiCo LDH	983.6 F g^{-1} (2 A g^{-1})	52.4% (50 A g^{-1})	76% (5000)	2
NiCo-SDBS-LDH	1094 F g^{-1} (5 A g^{-1})	41.3% (10 A g^{-1})	71% (3000)	3
Ag NW@NiAl LDH	1148 F g^{-1} (1 A g^{-1})	63.4% (10 A g^{-1})	77.2% (10000)	4
ZIF-8-C@NiAl-LDH	1370 F g^{-1} (1 A g^{-1})	77% (10 A g^{-1})	80% (1000)	5
$NiCo_2O_4$@NiCoAl-LDH nanoforests	1814.2 F g^{-1} (1 A g^{-1})	60.9% (20 A g^{-1})	93% (2000)	6
CoAl-LDH/FG-12	1222 F g^{-1} (1 A g^{-1})	75.3% (10 A g^{-1})	88.3% (3000)	7
Cactus-like NiCoP/NiCo-OH	1100 F g^{-1} (1 A g^{-1})	60% (10 A g^{-1})	90% (1000)	8
Ni-Al LDH hollow sphere	1578 F g^{-1} (1 A g^{-1})	56% (20 A g^{-1})	93.7% (10000)	9
NiAl-LDH nanoplates	1713.2 F g^{-1} (1 A g^{-1})	58% (5 A g^{-1})	88.7% (5000)	10
KCu_7S_4@NiMn LDH	733.8 F g^{-1} (1 A g^{-1})	76.9% (30 A g^{-1})	84.8% (16000)	11
MOF-derived Co-Co LDH	1205 F g^{-1} (1 A g^{-1})	60.3% (7 A g^{-1})	96.5% (2000)	12

Ni-Co LDH/GNR	1765 F g^{-1} (1 A g^{-1})	68% (20 A g^{-1})	83% (2000)	13
NCLP@NiMn-LDH	2312 F g^{-1} (1 A g^{-1})	65% (20 A g^{-1})	90% (10000)	This work

Table 2. The energy density of various electrodes in an ASC system in references

Asymmetric supercapacitor	**Energy density (maximum)**	**Ref**
Mxene-NiCo LDH//MWCNT	36.7 Wh kg^{-1}	2
NiCoP/NiCo-OH//PC	34 Wh kg^{-1}	8
NiAl-LDH//ACNF	20 Wh kg^{-1}	9
Ag NW@NiAl LDH// Ag NW@NiAl LDH	17.7 Wh kg^{-1}	10
KCu_7S_4@NiMn LDH//AG	15.9 Wh kg^{-1}	11
NiCo-LDH/3D rGO NF//AC	38.6 Wh kg^{-1}	12
Ni-Co LDH/GNR//AC	25.4 Wh kg^{-1}	13
G-NiAl-LDH//rGO	35.5 Wh kg^{-1}	14
rGo/CoAl-LDH//rGO	22.6 Wh kg^{-1}	15
NiP@CoAl-LDH NTAs//AC	37.8 Wh kg^{-1}	16
NCLP@NiMn-LDH//AC	42.2 Wh kg^{-1}	This work

Note and references

1. X. Li, L. Yu, G. Wang, G. Wan, X. Peng, K. Wang and G. Wang, *Electrochim. Acta*, 2016, **255**, 15-22.

2. H. Li, F. Musharavati, E. Zalenezhad, X. Chen, K. N. Hui and K. S. Hui, *Electrochim. Acta*, 2018, **261**, 178-187.

3. Y. Lin, X. Xie, X. Wang, B. Zhang, C. Li, H. Wang and L. Wang, *Electrochim. Acta*, 2017, **246**, 406-414.

4. L. Li, K. S. Hui, K. N. Hui, T. Zhang, J. Fu and Y. R. Cho, *Chem. Eng. J*. 2018, **348**, 338-349.

5. B. Han, G. Cheng, E. Zhang, L. Zhang and X. Wang, *Electrochim. Acta*, 2018, **263**, 391-399.

6. X. He, Q. Liu, J. Liu, R. Li, H. Zhang, R. Chen and J. Wang, *J. Alloys Compd.*, 2017, **724**, 130-138.

7. W. Peng, H. Li and S. Song, *ACS Appl. Mater. Interfaces*, 2017, **9**, 5204-5212.

8. X. Li, H. Wu, A. M. Elshahawy, L. Wang, S. J. Pennycook, C. Guan and J. Wang, *Adv. Funct. Mater.*, 2018, **28**, 1800036.

9. W. Wang, N. Zhang, Z. Shi, Z. Ye, Q. Gao, M. Zhi and Z. Hong, *Chem. Eng. J*., 2018, **338**, 55-61.

10. L. Li, K. S. Hui, K. N. Hui, Q. Xia, J. Fu and Y. Cho, *J. Alloys Compd.*, 2017, **721**, 803-812.

11. X. L. Guo, J. M. Zhang, W. N. Xu, C. G. Hu, L. Sun and Y. X. Zhang, *J. Mater. Chem. A*, 2017, **5**, 20579-20587.

12. X. Bai, J. Liu, Q. Liu, R. Chen, X. Jing, B. Li and J. Wang, *Chem. Eur. J.*, 2017, **23**, 14839-14847.

13. H. Jin, D. Yuan, S. Zhu, X. Zhu and J. Zhu, *Dalton Trans.*, 10.1039/C8DT01882K.

14. S. Wu, K. S. Hui, K. N. Hui and K. H. Kim, *ACS Appl. Mater. Interfaces*, 2017, **9**, 1395-1406.

15. R. Zhang, H. An, Z. Li, M. Shao, J. Han and M, Wei, *Chem. Eng. J.*, 2016, **289**, 85-92.

16. S. Wang, Z. Huang, R. Li, X. Zheng, F. Lu, T. He, *Electrochim. Acta*, 2016, **204**, 160-168.